

## DEVELOPMENT OF A COASTAL WAVE ENERGY CLIMATOLOGY

Jeff Hanson  
WaveForce Technologies LLC  
138 BayCliff Trail, Kill Devil Hills, NC 27948 USA  
Email: [Jeff4Waves@gmail.com](mailto:Jeff4Waves@gmail.com)

Kent K. Hathaway  
US Army Corps of Engineers, Field Research Facility  
Duck, North Carolina, USA

### ABSTRACT

A coastal wave energy climatology is developed based on a 35-year wave observation record obtained by the US Army Corps of Engineers at the Field Research Facility in Duck, NC. Spectral wave data from coastal observation stations ranging 6m to 26m in depth have been transformed using non-linear artificial neural net modeling to fill data gaps in a multi-decade time series at 18-m depth. A depth-dependant full spectral calculation of wave power shows Hurricane Isabel (2003) as the storm of record for maximum hourly wave power. Annual total wave energies depict a 3-5 year cycle, such occurs with major atmospheric cycles such as El Niño and the North Atlantic Oscillation. There are no obvious long term linear trends in the annual results. A coastal storm event chronology shows that nor'easters are the most frequent energetic storms, however the most powerful storms of the 35-year record are Hurricane Dennis (1999) followed by Hurricane Sandy (2012) and extratropical storm Nor'Ida (2009).

### 1. INTRODUCTION

There are increasing concerns over the effects of climate change on the coastal environment. Numerous offshore studies have investigated increases in North Atlantic storminess and wave heights (for example Bromirski and Kossin, 2008; Komar, 2007; Keim et al., 2004; The WASA Group, 1998; Kushnir et al., 1997). It is conceivable that both sea level rise and increasing storminess would contribute to increased coastal wave energy and hence accelerated coastal erosion (Bromirski and Kossin, 2008; Keim et al., 2004). However a scarcity of long-term data on coastal wave climates and corresponding geomorphologic responses makes it difficult to investigate the influence of storm event sequences and long-term wave climate on our coastlines.

Unlike the coastal environment, there are multiple data sets available for use in offshore wave climate studies. In general past studies of North Atlantic offshore wave climate show strong correlations

between wave energy and established climate indicators. An investigation of hurricane season wave observations along the US Atlantic and Gulf coasts from 1980 through 2006 indicates that Tropical Cyclone (TC) generated wave power increased during the last 10 years of the study period (Bromirski and Kossin, 2008) and appears to be modulated by the Atlantic Meridional Mode (AMM), which modulates TC frequency (Chiang and Vimont, 2004). Furthermore Bromirski and Kossin found a strong correlation between open-ocean and coastal wave power, however the coastal buoys employed were mostly on the outer shelf and hence a significant distance offshore. A 57-year hindcast of the northeast Atlantic wave climate (Dodet et al., 2010) reveals significant multi-year modulations correlated with the North Atlantic Oscillation (NAO), with the strongest correlations coming from higher latitudes.

Long-term data in the Atlantic coastal environment has been obtained by the US Army Corps of Engineers (USACE) through a coastal field data collection program starting in 1980 at the Field Research Facility (FRF) in Duck, North Carolina. As depicted in Figure 1, The FRF is situated on an open sandy coast and subject to the energetic wind and wave environment of the mid-Atlantic Ocean. Initial measurements included winds, waves and morphologic surveys.



Figure 1. US Army Corps of Engineers Field Research Facility, located on the open coast of North Carolina.

Data collected at the FRF from 1980-1998 from non-directional and directional Waverider buoys and an 8m depth pressure gauge array (Long and Shay, 1991)

were used to investigate the influence of storm groups on nearshore morphologic change (Lee et al., 1998; Birkemeier et al., 1999). These studies produced a near-continuous wave height and period record by filling gaps in an 18-m Waverider record with data from an 8m pressure array, without any wave depth transformations applied. The resulting wave record was used in a deep-water wave energy calculation to compute integrated wave power of key storm events. The results were used to demonstrate the importance of storm sequences in long-term morphologic change.

The FRF measurements program has evolved over time with increased sampling frequency, new measurement types, and additional stations. In 1996 the non-directional Datawell Waverider was changed to a directional and starting in 2008 a cross-shore array (XShore) of wave and current sensors was added with station depths ranging from 2-26m (Hanson et al., 2009). However, as with most field measurements, sporadic data gaps exist in the wave data from any given station. Data gaps are detrimental to a long-term climate analysis, as critical wave events can be missed resulting in erroneous mean and total wave energy calculations. A potential solution is to fill data gaps with wave data that has been depth-transformed from other FRF measurement stations. The challenge is that the nearshore wave climate at Duck can become strongly nonlinear (Hanson et al., 2009).

There are a variety of approaches that can be used to transform wave data between different stations and depths to fill data gaps. To accurately compute wave power, the spectral wave density is required, as bulk wave height and period parameters can overestimate wave power by 65% (Defne et al., 2009). One option is to use a packaged spectral wave model, such as STWAVE-FP (Smith, 2007) or SWAN (Holthuijsen, 2007). However as the source terms are primarily based on linear wave theory, spectral modeling performance at Duck has been shown to be compromised when the waves become strongly nonlinear (Hanson et al., 2009). A second option is that of a phase-resolving wave model, such as CGWAVE (Demirbilek and Panchang 1998). However phase resolving models can be computationally intensive for a 35-year hindcast. Finally we consider non-linear Artificial Neural Network (ANN) modeling. Neural nets have been used successfully in a variety of wave transformation applications, including the estimation of swell in coastal regions (Browne et al.,

2007), and the translation of satellite wave data to coastal locations (Kalra et al., 2005). More recently, Alexandre et al. (2015) applied an artificial learning multi-station approach for offshore buoy data gap filling. However the vast majority of these studies focused on the transformation of the bulk wave parameters (height, period and direction) rather than the full wave energy density spectra which is needed for the accurate calculation of wave power.

Here we develop and apply ANN techniques for transforming the FRF wave spectra between stations, allowing for the creation of nearly gap-free 35-year series of wave spectra. Furthermore we employ depth-dependant spectral wave power calculations to describe the coastal wave energy climate.

## 2. DATA

The wind and wave data used in this study were obtained from US Army Corps of Engineers during 1980-2014 by observation stations included in a 16.4-km cross-shore wave and current array (XShore) at the FRF in Duck, North Carolina. As depicted in Figure 2, XShore includes Datawell Waverider buoys at 18- and 26-m depths, 4 bottom mounted Nortek Acoustic Wave and Current (AWAC) sensors at 6-11 m depths, and an 8m depth pressure gage array. An instrument tower at the end of the FRF pier (7-m water depth) includes a meteorological station with a marine anemometer (currently RM Young Model 09101) located at an elevation of 19.1 m NAVD88. Specific details on each measurement station appear in Table 1. All data sets contain gaps due to incomplete records or sensor/mooring malfunctions. The amount of good data for each station, based on an hourly record count, appears in the last column of Table 1.

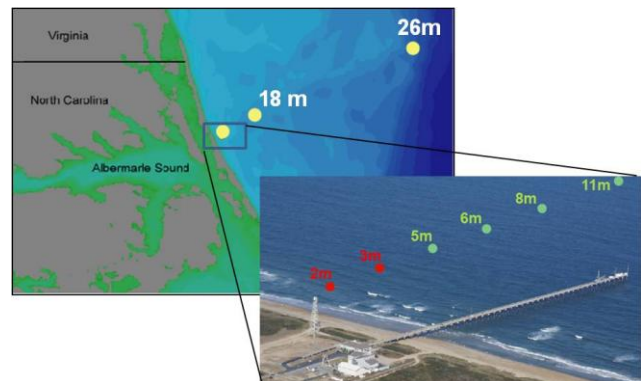


Figure 2. FRF Wave measurement stations

**Table 1. FRF Measurement Stations used for Wave Energy Study**

Station	Instruments	Nominal Depth / Elevation (m,NAVD88)	Cross-shore Distance (km)	North Latitude	West Longitude	Telemetry	Placed in Service	Removed from Service	Good Data
6m	1000 kHz AWAC	-6.8	0.60	36.1873	75.7465	Cable	Sep 2008	ongoing	82%
8m	1000 kHz AWAC	-8.7	0.90	36.1882	75.7432	Cable	Sep 2008	ongoing	75%
8m	Directional Pressure Array	-8.2	0.90	36.1872	75.7428	Cable	Sep 1990	Oct 2012	95%
11m	1000 kHz AWAC	-11.5	1.20	36.1892	75.7392	Cable	Sep 2008	ongoing	72%
18m	Non-Directional Waverider	-17.1	3.60	36.1999	75.7141	HF	Oct 1980	Oct 1996	45%
18m	Directional Waverider	-19.3	3.60	36.1999	75.7141	HF/Iridium	Nov 1996	ongoing	93%
26m	Directional Waverider	-26	16.40	36.2577	75.5913	Iridium	Jun 2008	ongoing	83%
FRF Pier	Anemometer	19.6	0.60	36.1837	75.7451	Cable	Sep 1987	ongoing	68%

The data set includes all major coastal storms and hurricanes that have influenced the region in the past 35 years. A sample 6-year wave height record (2008-2014) from the 18m station appears in Figure 3. Selected named tropical storms and significant nor'easter events are identified. The storm of record for this period was Hurricane Sandy, with significant wave heights ( $H_s$ ) greater than 6m. Data from multiple XShore stations during Hurricane Sandy appear in Figure 4. Note that the 11m station was non-operational during this storm, and a 2m depth station, not used in this study, is included in the figure. The significant wave height records (lower panel) show the evolution of the wave field at each of the included

stations. A distinct tidal signature can be seen in the 2m wave heights. Example energy-density spectra (upper left panel) compare the wave spectra at each station during the storm peak. The transformation of normalized wave energy across the array, as a function of  $kd$  where  $k$  is the peak wavenumber and  $d$  is the depth, appears in the upper right panel. Note that there is significant loss of energy by breaking across the array during large storm events (Hanson et al., 2009). Hence the data from one station cannot be directly used to fill gaps in the data from another station. Specific details on the preparation of these data follow below.

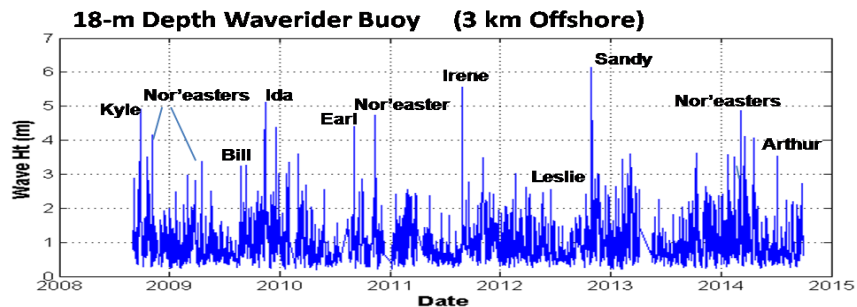


Figure 3. Sample significant wave height record from 18m Waverider buoy, with identification of significant storm events.

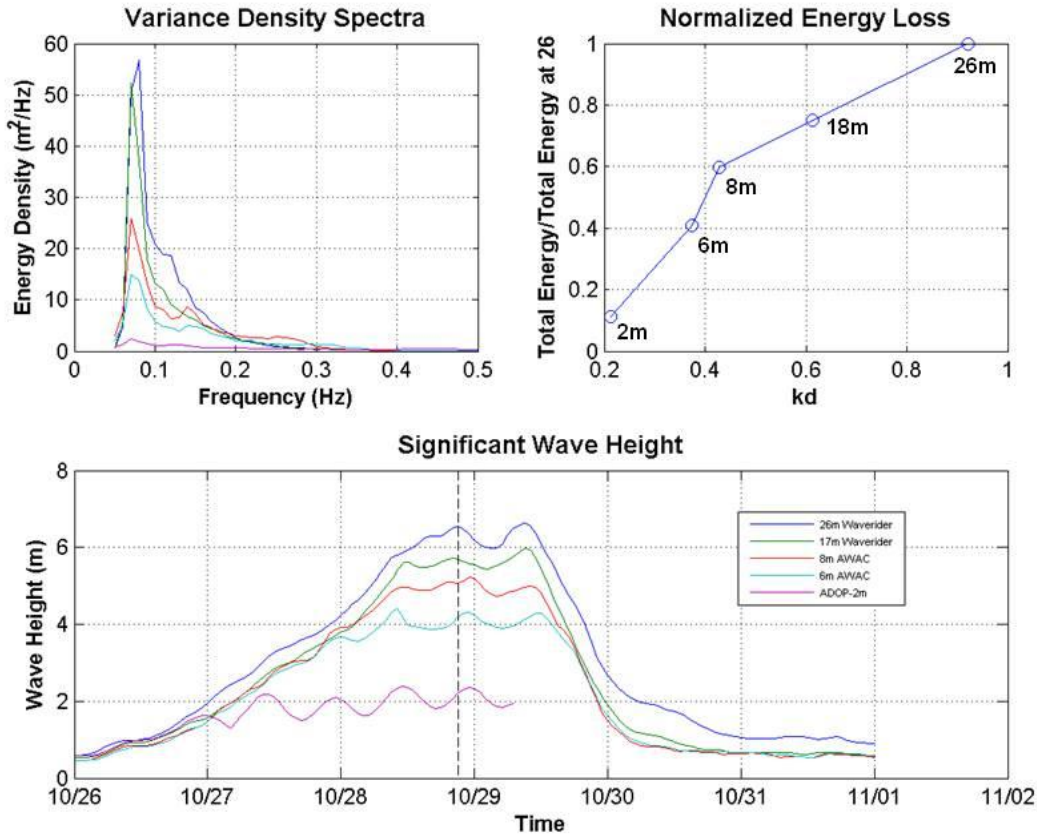


Figure 4. FRF XShore array data from Superstorm Sandy including wave height time series (lower panel), non-directional wave spectra during storm peak (upper left), and normalized energy loss across the array during storm peak (upper right).

### 2.1. Wind Measurements

Wind measurements were used in this study to help separate local wind sea from swell (see Wave Measurements). The FRF wind measurements were collected by a variety of sensors allowing for redundancy in the event of sensor failure. In 2014 a study was undertaken to develop a set of ‘best winds’ for this historical record. Applying stringent quality assurance/quality control (QA/QC) standards, the raw data records were evaluated and filtered to identify and prepare the best records for representing the winds during each 10-minute observation time. The selected records were used to compute a near-continuous series of 10-minute average winds (vector averaging for directions). Data gaps occur for time periods when all wind sensors were inoperative or when no data sets passed the QA/QC criteria. The resulting 10-minute winds were forward-averaged to create 30-minute average winds which approximately correspond to the wave buoy data collection periods.

### 2.2 Wave Measurements

Several steps were required to prepare the wave data for long-term evaluation of wave climate. Data collection procedures for the various sensors are described by Hanson et al. (2009). Spectra were computed from approximately 30 minute wave records (60 minute for 8m pressure array) using the Iterative Maximum Likelihood Method (Oltman-Shay and Guza, 1984). Further preparation and analysis of the resulting wave spectra was performed using the WaveForce Technologies XWaves ocean wavefield analysis toolbox (Hanson and Fratantonio, 2015). These data preparation steps included:

*Smoothing*- A 3-hour weighted smoothing algorithm was applied to all spectral data. This helps to reduce noise and results in a more efficient partitioning of sea and swell parameters (see Transformation Modeling).

*Interpolation* – The energy-density spectra were interpolated to a uniform set of frequency bins from 0.05 – 0.5 Hz at 0.01 Hz resolution. Due to array

configuration and pressure response, the 8m pressure array spectra have a high-frequency cut off of 0.35 Hz. Directional spectra were interpolated to 36 angle bins (0-350 deg) at 10-deg resolution. Such interpolations significantly improve the spectral partitioning results (see below).

*Spectral tails* – Spectral tails out to 0.5 Hz were added to the 8m pressure array spectra using the Ochi-Hubble model (Ochi and Hubble, 1976) blended over 4 overlapping frequency bins. The  $\cos^{2n}$  directional distribution of the highest observed spectral bin was used in the tail region.

*Subsetting* – The resulting spectral files for each station were subset to 1-hour resolution.

*Wind interpolation* – The 30-min forward-averaged winds were vector interpolated to match the wave record observation times. No interpolations were performed in wind data gaps larger than 3 h in duration. For the wind data gaps, wind speed and directions were estimated based on properties of the observed wave spectra (Hanson et al., 2010).

The above procedures have resulted in a consistent set of wave spectra from each XShore station. Based on hourly record counts, the amount of good data from each of these stations is reflected in the last column of Table 1.

### 3. TRANSFORMATION MODELING

To generate a near-continuous wave record at any given station we fill in data gaps using transformed data from the other XShore stations. As stated previously, spectral information must be transformed to facilitate accurate calculation of wave energy over changing bottom depths. As the 18-m station contains the longest series of data (non-directional and directional), we have selected this as our target location for the present study.

We employ an ANN approach to develop a multi-dimensional non-linear fit of wave observations at the various XShore stations to wave observations at the 18m station. The method is based on a two-layer feed-forward network with  $i$  hidden neurons or layers. A set of inputs with known outputs are used to train the nets using the Levenberg-Marquart back-propagation algorithm (Marquardt, 1963). Performance is evaluated using mean square error and regression analysis.

This approach employed the following data preparation and modeling steps:

- Reduce wave spectra to a minimum set of parameters
- Develop a training set of wind and wave parameter inputs and known wave outputs (targets)
- Train nets and evaluate performance
- Apply trained nets to transform XShore station data to fill 18m station gaps

The entire process was iterative, in order to identify the optimum set of wind and wave parameter inputs to yield the best possible ANN performance. Details are provided in the following sections.

#### 3.1. Spectral Parameters

Our initial attempts to transform the entire directional wave spectral matrix in a single neural net model yielded unsatisfactory results; transformed spectra had significantly higher noise levels than the original data. Hence we adopted an approach using a reduced set of wave spectral parameters, based on wave partitioning of sea and swell wave systems and spectral fitting with spectral shape models.

Wave partitioning in XWaves uses an inverse watershed algorithm to isolate peak domains in directional wave spectra (Hanson and Fratantonio, 2015; Hanson and Phillips, 2001). An iterative smoothing approach (Portilla et al., 2009) has been incorporated to successively combine neighboring peaks until the number of wave components is less than or equal to maximum threshold set by the user. Wind sea peaks are identified using a directional wave age criterion (Hanson and Phillips, 2001). Statistics computed for each partition include  $H_s$ , peak period ( $T_p$ ), and mean wave direction ( $D_m$ ). Resulting sea and swell energy-frequency spectra are fit with the Ochi-Hubble model which yields the spectral shape parameter ( $\lambda$ ). Partition directional distributions are fit with a  $\cos^{2n}$  model yielding the distribution parameter  $2n$  (DNV, 2010; see equation 3.5.8.4). Hence each spectral partition is described by 5 fit parameters ( $H_s$ ,  $T_p$ ,  $D_m$ ,  $\lambda$ , and  $2n$ ). For the FRF wave energy study, the analysis was set to produce no more than three wave partitions at each time step. Example partition and fit results appear in Figure 5.

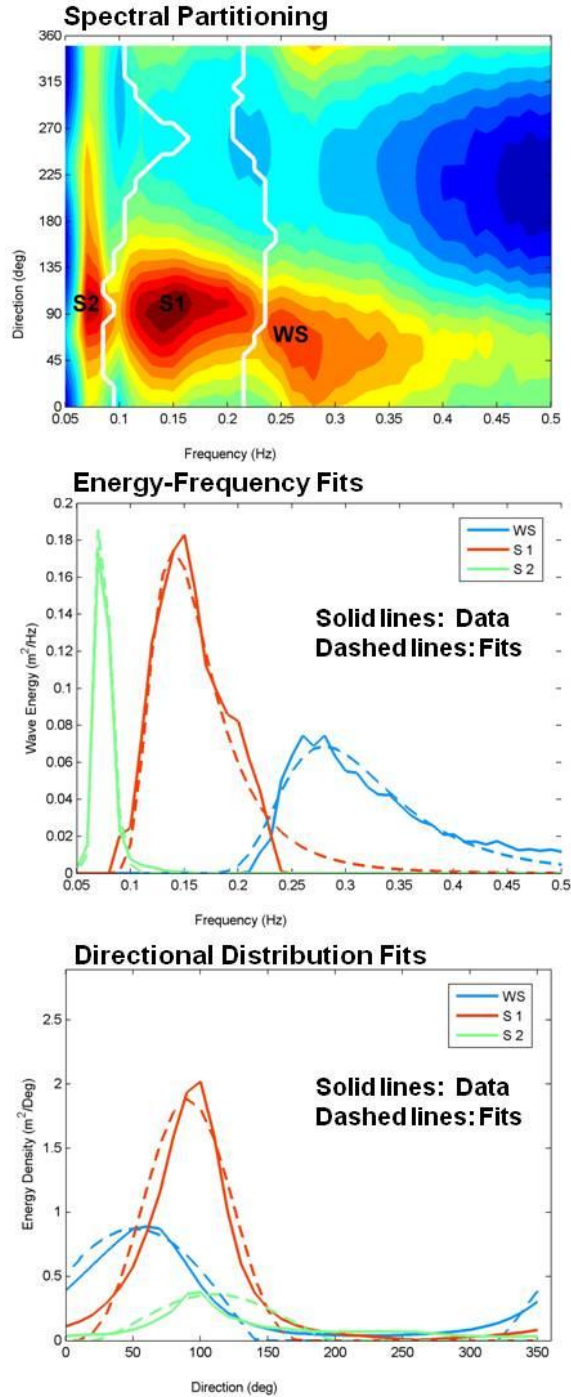


Figure 5. Sample spectral partitioning and fitting of observations at 18m station on 1 October 2014. Upper panel: Directional wave spectrum partitions with sea (WS), dominant swell (S1) and secondary swell (S2); Middle panel: Energy frequency fits with Ochi-Hubble model; Lower Panel: Directional distribution fits with  $\cos^{2n}$  model.

### 3.2. Model Development

In comparing XShore station data sets it was determined that 2009 contained the most complete set of records across the array. Therefore, the wave data from 2009 was initially selected as our ANN training set. After testing, it was determined that a single year did not contain sufficient representation of peak wave height events. Hence, the data from all wave events with  $H_s > 2.5$  standard deviations above the mean during 2008-2014 were added to the 2009 training set. As will be demonstrated, the resulting combined training set provides adequate representation of the FRF wavefield variability.

Separate ANN models were trained for each of the 5 spectral fit parameters. Our output (target) was the 18m wave climate. The inputs to each model included fit parameters computed for all remaining XShore stations (26m, 11m, 8m, and 6m). To better handle wave direction transitions across 0 deg (North), the mean wave directions were split into north and east components:

$$D_n = \cos\left(\frac{\pi D_m}{180}\right),$$

$$D_e = \sin\left(\frac{\pi D_m}{180}\right).$$

Due to the uniqueness of the 8m pressure array station, a separate set of ANN fit parameter models were generated for this station. The specific input parameters selected for each model, along with the number of hidden layers employed, appear in Table 2. Note that  $T_p$  was highly correlated across stations; hence this model was replaced by setting  $T_p$  constant across the array for any given wave partition. By including the nominal station depth  $h$  as an input parameter, each of the parameter models handled wave propagation in both directions; shoreward from the 26m station and back-propagating seaward from the nearshore stations.

Table 2. Artificial Neural Net Model Configurations

Model Target	Input Parameters	Hidden Layers $i$
Hs	$H_s, T_p, D_n, D_e, h$	6
Tp	$T_p$	1
Dm	$T_p, D_n, D_e, h$	12
$\lambda$	$H_s, T_p, D_n, D_e, \lambda, h$	14
2n	$T_p, D_n, D_e, 2n, h$	6

The trained nets were used to transform spectral fit parameters from the original station locations to the 18m station. The Ochi-Hubble and  $\cos^{2n}$  models were employed to reconstruct wave partition spectra from the transformed fit parameters. The resulting partition spectra from each time step were summed to regenerate full directional wave spectra. Sample reconstructed spectra appear in Figure 6. Note that these are the same spectra used to demonstrate the partitioning and fitting process in Figure 5.

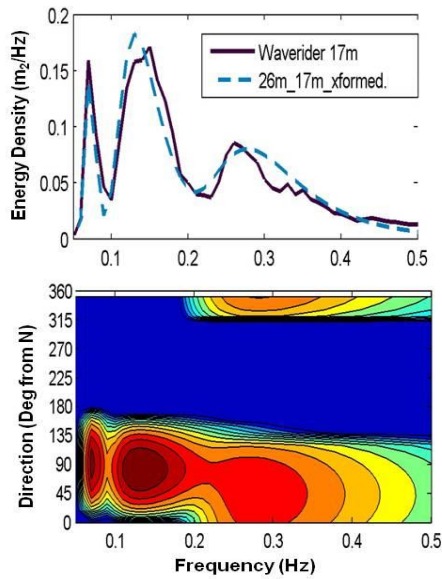


Figure 6. Comparison of 18m observed and 26m transformed spectra from 1 October 2014. Upper panel: Energy-frequency spectra; Lower Panel: Reconstructed directional spectrum from 26m station.

A full validation is performed by comparing the transformed reconstructed 18m spectra to the actual measurements at this location. The 26m and 6m station  $H_s$  validations appear in Figure 7. All available data are included. The left panels show how the 26m and 6m station  $H_s$  data compared to the 18m station data prior to transformation. The right panels show the results of the transformation. The transformed data exhibit essentially a zero bias ( $b$ ), and in the case of 26m, greatly reduced RMS error ( $Erms$ ). The higher  $Erms$  at the shallow station is likely a combination of factors, including (1) it is the station with the most depth change from 18m, the existence higher instrument (acoustic sonar) noise levels in the surf zone, and (3) as a result of the shallow depth, the wavefield is most nonlinear at this station.

### 3.3. Gap Filling

Transformed and reconstructed spectra were used to fill in data gaps in the 18m station data. We define a data gap as any time period persisting for 1 h or greater without a valid wave record. The priority order of stations for filling the gaps appears in Table 3. Also provided are statistics on the amount of data used from each station. Once all the directional wave stations were used, the 18m non-directional Waverider set was used for any remaining gaps. As the non-directional Waverider data come from the 18m location, data transformation was not required. Approximately 27% of the data in the resulting long-term wave record were transformed from other depth stations.

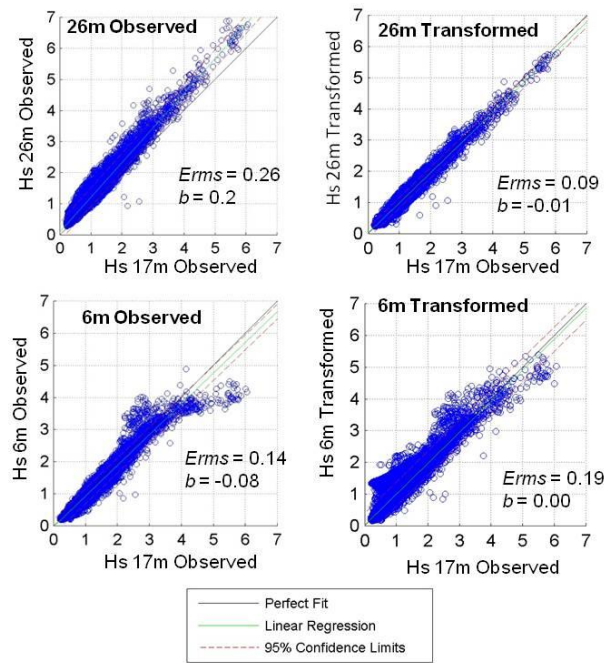


Figure 7. Validation of neural net modeling results at 26m and 6m stations. Left panels depict original station  $H_s$  compared to 18m wave  $H_s$ . Right panels compare transformed station  $H_s$  to 18m  $H_s$ . The RMS error ( $Erms$ ) and bias ( $b$ ) are provided for each regression.

Table 3. Data Sources for 18m Long-Term Record

Source (in priority order)	# Records
18m Directional Waverider	146,814
26m Waverider	4,841
11m AWAC	697
8m AWAC	245
6m AWAC	173
8m Array	56,648
18m Non-directional Waverider	24,751
Total	234,169

#### 4. WAVE ENERGY CLIMATOLOGY

Although wave height and period are traditionally looked at in terms of coastal wave climatologies, wave power is ultimately responsible in moving coastal sediments, driving electrical power generators, promoting air-sea exchange, mixing the water column and even providing the required push for recreational surfing. Hence we focus on wave power and total energy considerations.

##### 4.1. Wave energy calculations

The depth-dependant full spectral wave power calculation (Defne et al., 2009) is given by

$$P = \rho g \int S(f) \cdot C_g(f) \cdot df,$$

with water density  $\rho$ , gravitational acceleration  $g$ , and wave group velocity

$$C_g = \frac{\omega}{2k} \left( 1 + \frac{2kh}{\sinh(2kh)} \right),$$

where  $\omega$  is the radian wave frequency,  $k$  is the radian wave wavenumber, and  $h$  is the water depth. The solution for  $C_g$  must be found iteratively, as there are unknowns on both sides of the equation.

Wave power was computed for each record in the gap-filled 18m data set. The results were then interpolated to even hour increments. Interpolations were not performed over data gaps longer than 6 h. Based on an hourly record count, unresolved gaps comprised only 6% of the resulting interpolated data set.

Average and total energy calculations were performed over each month and each year of the gap-filled data set. The average wave power is simply the average of  $P$  over the time period of interest. The total wave energy is given by

$$E_t = \int P dt.$$

Furthermore the total energy of significant storm events was calculated. Storm events are defined after Birkemeier et al. (1999), as an event with  $H_s > 3.0m$ . Storm duration is determined from the time that the wave height exceeded 3.0m until the height fell below 2.35m (which was the mean wave height plus two times the standard deviation in the Birkemeier et al. study).

##### 4.2 Climate trends

The hourly wave power record for the 18m station, shown in Figure 8, depicts a pattern of extreme wave power events over the study duration. Hurricane Isabel (2003) is the storm of record (35-years) with a

maximum hourly wave power of 311 kW/m. Other significant events include Hurricanes Gloria (1985) and Sandy (2012) which exhibited  $>200$  kW/m hourly wave power. Inspection of wave power events rising above 150 kW/m suggests that the frequency of occurrence has increased in the past decade.

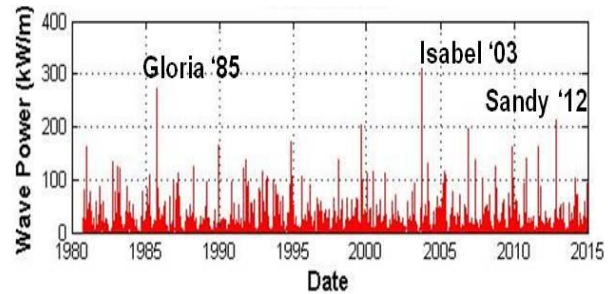


Figure 8. Hourly gap-filled wave power record for the 18m depth station.

The long-term record was used to compute monthly average wave power for the 35-year period. The results, depicted in Figure 9, show the dramatic changes that occur over the course of a year. Average wave power is lowest in July, increases by a factor of 4 by September, and remains at high levels through March. For 6 months each year the monthly average wave power rises above 6 kW/m.

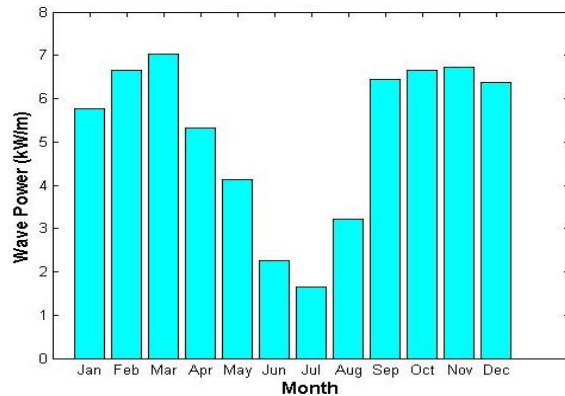


Figure 9. Average monthly wave power computed over 1981 through 2014 at 18m depth.

Long-term trends are revealed by annual wave energy and wave power statistics. Annual variability in average wave power, appearing in Figure 10 (lower panel) suggests a 3-5 year cycle. This trend is strongly evident in the annual total wave energy, appearing in Figure 10 (upper panel). In particular from 1990 through 2010 there is strong evidence of a 3-5 year cycle in annual total wave energy. Such sequences are likely driven by major atmospheric cycles such as El Niño Southern Oscillation and the North Atlantic Oscillation (NAO), which are both known to influence storm activity in

the Atlantic. Neither the average power nor total energy statistics show any discernible long term trends towards increasing or decreasing coastal wave energy conditions.

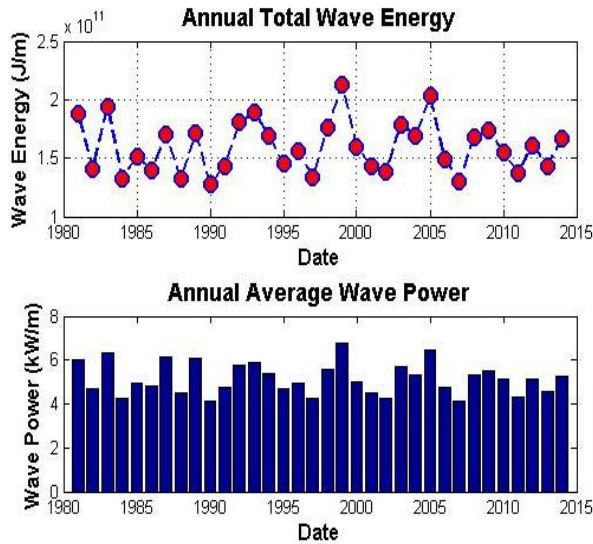


Figure 10. Annual total wave energy (upper panel) and average wave power (lower panel) based on the gap-filled record at 18m depth.

Of particular interest is the storm event chronology, as this an important indicator of wave-induced coastal change (Birkemeier et al., 1999). A 35-year storm history appears in Figure 11. The total storm energy (upper panel) essentially updates Figure 5 in Birkemeier et al. (1999). Total storm duration (lower panel) is included for reference as total storm energy is obtained by integrating the wave power over the entire storm duration (see Wave Energy Calculations above). The most energetic storm events are labeled, and it should be noted that the storms that produce the highest hourly wave power values (Figure 8), are not necessarily the most energetic storms. Although most of the long-duration / high wave energy events are nor'easters, the overall storm event of record is Hurricane Dennis (1999), with 100 h (4-day) duration of high power waves. Other high-energy events include Hurricanes Sandy (2012) and extratropical storm Nor'ida (2009). Note that Hurricane Isabel (2003), which was our hourly wave power storm of record (Figure 8), is only the eighth most energetic storm on record for this period, with a 40-h duration. Linear regressions on both storm power and storm duration show slight increases over time; however data scatter is high and confidence in the result is low.

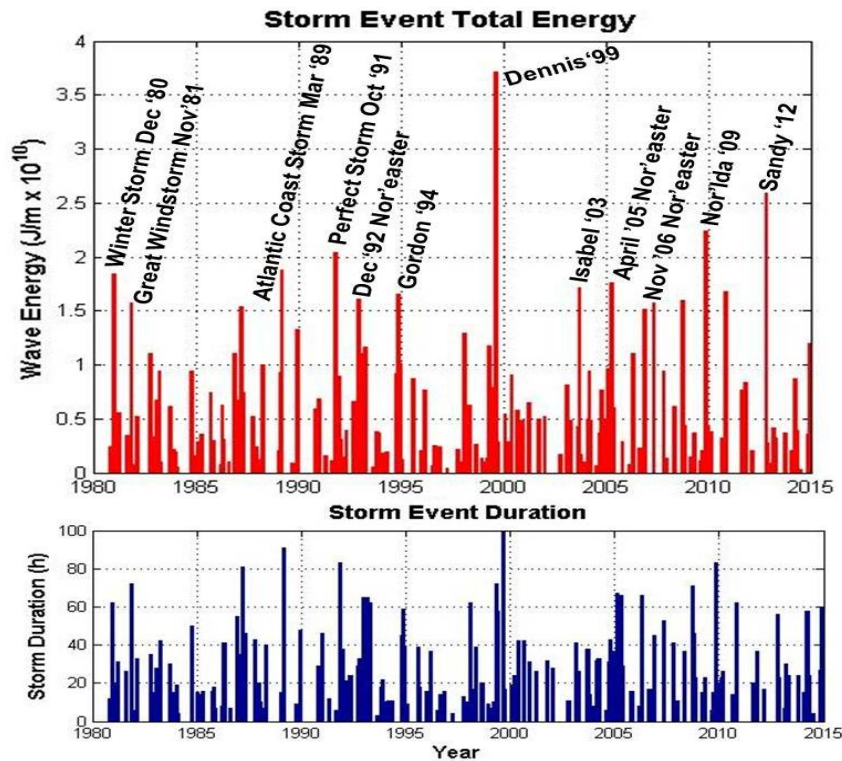


Figure 11. Storm event total energy (upper panel) and duration (lower panel) based on the gap-filled record at 18m depth.

## SUMMARY

The 35-year wave climate in a dynamic coastal setting is described. Using records from multiple wave observation stations at the USACE Field Research Facility in Duck, NC, a near continuous coastal wave record is developed at 18m depth. To fill critical data gaps, wave spectral parameters are transformed between cross-shore measurement stations ranging from 8m to 26m in depth. The transformations are accomplished using a non-linear artificial neural net modeling approach. The resulting 35-year hourly wave spectrum record is 94% complete with data gaps occurring only 6% of the time.

The wave spectrum record is used to describe the nearshore wave power and energy climate. A fully depth-dependant spectral calculation of wave power provides an accurate assessment of nearshore wave power. Hourly wave power depicts the frequency and intensity of large wave events over the 35-year record. Hurricane Isabel (2003) is the storm of record for maximum hourly wave power. The results suggest that the frequency of occurrence of high-power wave events has increased in the past decade. Annual statistics depict a 3-5 year cycle, which is most prevalent in annual total wave energy. Such cycles are likely driven by major atmospheric cycles (including El Niño and NAO), and additional work is underway to investigate this cyclic behavior. There are no obvious long term linear trends based on the annual statistics.

Finally a coastal storm event chronology is presented for the 35-year period. Comparisons with Birkemeier et al. (1999) show decreased event energies as a result of an improved calculation of coastal wave power. Storms that produce the highest hourly wave power are not necessarily the most energetic events. Although nor'easters dominate most of the storm event record, Hurricane Dennis (1999), persisting for 100 h, is the most energetic storm of the period.

Ongoing work is focused on describing the coastal wave climatology in terms of sea and swell sources.

## ACKNOWLEDGEMENTS

All data provided by the US Army Corps of Engineers Coastal Observations and Analysis Branch (COAB). We appreciate numerous insightful discussions with Dr. Kate Brodie, Mr. Michael Forte, and Dr. Jesse McNinch. Initial inspiration for the project was provided by Mr. William Birkemeier. Funding for Dr. Hanson provided by COAB through RPS Evans Hamilton, Inc.

## REFERENCES

- Alexandre, E., L. Cuadra, J.C. Nieto-Borge, G. Candil-García, M. del Pino, and S. Salcedo-Sanz, 2015. A hybrid genetic algorithm—extreme learning machine approach for accurate significant wave height reconstruction, *Ocean Modelling*, 92, 115-123.
- Birkemeier, W.A., Nicholls, R.J. and Lee, G., 1999. Storms, storm groups and nearshore morphologic change, *Coastal Sediments '99*. ASCE Press, Long Island, NY.
- Bromirski, P.D., and J. P. Kossin, 2008. Increasing hurricane wave power along the U.S. Atlantic and Gulf coasts, *J. Geophys. Res.*, 113 (C07012), 10 pp.
- Browne, M, B. Castelle, D. Strauss, R. Tomlinson, M. Blumenstein, and C. Lane, 2007. Near-shore swell estimation from a global wind-wave model: Spectral process, linear, and artificial neural network models, *Coastal Engineering*, vol. 54, no. 5, pp. 445-460.
- Chiang, J.C.H., and D. J. Vimont, 2004. Analogous Pacific and Atlantic meridional modes of tropical atmosphere-ocean variability, *J. Clim.*, 17, pp. 4143-4158.
- Defne, Z., K. A. Haas and H. M. Fritz, 2009. Wave power potential along the Atlantic coast of the southeastern USA, *Renewable Energy*, 34, pp. 2197-2205.
- Dodet, G., X. Bertin and R. Taborda, 2010. Wave climate variability in the North-East Atlantic Ocean over the last six decades, *Ocean Modelling*, 31, (3-4), 2010, pp. 120-131
- DNV, 2020. Environmental Conditions and Environmental Loads, Recommended Practice DNV-RP-C205, DET NORSKE VERITAS, 124 p.
- Hanson, J.L., and R. Fratantonio, 2015. XWaves 6.0 Users Guide, online manual, WaveForceTechnologies, <http://waveforcetechnologies.com/help/index.html>.
- Hanson, J.L., A. Lübben, P. Aalberts and M. L. Kaminski, 2010. Wave Measurements for the Monitas System, Offshore Technology Conference 2010, OTC 20869, 12 p.
- Hanson, J.L., H.C. Friebel and K.K. Hathaway, 2009. Coastal Wave Energy Dissipation: Observations And STWAVE-FP Performance, 11TH International

- Workshop on Wave Hindcasting and Forecasting; Halifax, Nova Scotia, Canada; October 18-23, 2009.
- Hanson, J.L. and Phillips, O.M., 2001. Automated analysis of ocean surface directional wave spectra, *J. Atmos. Oceanic Technol.*, 18, pp. 277-293.
- Ho, P-C., and J. Yim, 2005. A study of the data transferability between two wave-measuring stations, *Coastal Engineering*, 52 (4), pp. 313-329.
- Holthuijsen, L.H., 2007. *Waves in Oceanic and Coastal Waters*, Cambridge University Press, 387 pp.
- Kalra, R., M.C. Deo, R. Kumar and V. K. Agarwal, 2005. Artificial neural network to translate offshore satellite wave data to coastal locations, *Ocean Engineering*, 32, pp. 1917-1932.
- Keim, B.D., R. A. Muller, and G. W. Stone, 2004. Spatial and temporal variability of coastal storms in the North Atlantic Basin, *Mar. Geol.*, 210, pp. 7-15.
- Komar, P.D., 2007. Higher waves Along U.S. east coast linked to hurricanes, *Eos*, 88, (30), pp. 301-308.
- Kushnir, Y., V. J. Cardone, J. G. Greenwood and M.A. Cane, 1997. The recent increase in North Atlantic wave heights, *J. Clim.*, 10, pp. 2107-2113.
- Long, C. E., and Oltman-Shay, J.M., 1991. Directional characteristics of waves in shallow water, Technical Report CERC-91-1, US Army Engineer Waterways Experiment Station, Vicksburg, MS.
- Marquardt, D. W., 1963. An algorithm for least-squares estimation of nonlinear parameters, *J.Soc. Indus. App. Mathematics*, 11(2), pp. 431-441.
- Ochi, M.K. and E. N. Hubble, 1976. On six-parameter wave spectra, Proc. 15th Conf. Coastal Engng., Vol.1, pp301-328.
- Oltman-Shay, J. M., and R. T. Guza, 1984. A data adaptive ocean wave directional-spectrum estimator for pitch and roll type measurements, *J. Phys. Oceanogr.*, 14, pp. 1800-1810.
- Panchang, V. G., & Z. Demirbilek. 1998. CGWAVE: A Coastal Surface Water Wave Model of the Mild Slope Equation, U S Army Waterways Experiment Station, Technical Report CHL-98-26, September, 1998, p. 118
- Portilla, J., F. O. Torres, and J. Monbaliu, 2009. Spectral partitioning and identification of wind sea and swell, *J. Atmos. Oceanic Technol.*, 26, pp. 107-122.
- Smith, J.A., 2007. Full-Plane STWAVE with Bottom Friction: II. Model Overview, US Army Corps of Engineers, Engineer Research and Development Center Technical Report ERDC/CHL CHETN-1-75, 15p.
- The WASA Group, 1998. Changing waves and storms in the Northeast Atlantic?, *Bull. Amer. Met. Soc.*, 79 (5), pp.741-760.